

Transient analysis of luminescent coupling effects in multi-junction solar cells

Takeshi Tayagaki, S. Kasimir Reichmuth, Henning Helmers, and Gerald Siefer

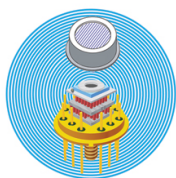
Citation: *Journal of Applied Physics* **124**, 183103 (2018); doi: 10.1063/1.5046543

View online: <https://doi.org/10.1063/1.5046543>

View Table of Contents: <http://aip.scitation.org/toc/jap/124/18>

Published by the [American Institute of Physics](#)

Ultra High Performance SDD Detectors



See all our XRF Solutions

Transient analysis of luminescent coupling effects in multi-junction solar cells

Takeshi Tayagaki,^{1,2,a)} S. Kasimir Reichmuth,¹ Henning Helmers,¹ and Gerald Siefer¹

¹Fraunhofer Institute for Solar Energy Systems (ISE), Heidenhofstr. 2, 79110 Freiburg, Germany

²Research Center for Photovoltaics, National Institute of Advanced Industrial Science and Technology (AIST), Tsukuba, Ibaraki 305-8568, Japan

(Received 28 June 2018; accepted 27 October 2018; published online 13 November 2018)

We investigate the luminescent coupling (LC) effects in a four-junction GaInP/GaAs//GaInAsP/GaInAs concentrator solar cell based on transient open-circuit voltage (V_{oc}) measurements under monochromatic illumination. Photocurrent generation in the non-absorbing GaInAs bottom subcell due to LC from upper subcells shows superlinear behavior with increasing light intensity. Along with this, a V_{oc} enhancement is observed and quantified for illumination intensities that span almost six orders of magnitude. The V_{oc} increase is explained and studied using a series-connected diode model including subcell shunt resistances, capacitances, and LC effects. The impact of unilluminated subcells on the subcell V_{oc} determination is discussed for multi-junction solar cells. Finally, in the analysis of the LC generated photocurrent, namely, the coupling factor from the GaInAsP to the non-absorbing GaInAs subcell, a characteristic dependency on bias voltage is shown and explained by a result of competing photo- and electroluminescence mechanisms. *Published by AIP Publishing.* <https://doi.org/10.1063/1.5046543>

I. INTRODUCTION

The luminescence properties, especially the radiative recombination processes, of solar cells have attracted much attention for the fabrication and characterization of high-efficiency solar cells.^{1–3} Photon recycling has shown to enable significant raise in the conversion efficiency of thin GaAs solar cells.^{4–10} Multi-junction solar cells show the highest conversion efficiency from solar irradiation to electricity under concentrated light irradiation.¹¹ Luminescent coupling (LC) between subcells has been extensively studied in stacked series-connected multi-junction devices.^{1,12–16} Photon recycling originates from the re-absorption of luminescence (i.e., photons generated by radiative recombination); luminescent coupling is considered a specific case of photon recycling where luminescence from radiative recombination in higher-bandgap subcells is re-absorbed by lower-bandgap subcells beneath. As a consequence, LC increases the photocurrent in the lower-bandgap subcell. Therefore, if one of the lower-bandgap subcells limits the current in a series-connected multi-junction solar cell, LC can counteract this limitation and, thus, increase the current of the overall device. Thereby, effective LC improves the annual yield of multi-junction solar cells for terrestrial applications,¹⁷ namely, by compensating for current mismatch in spectral mismatch conditions.²

LC also affects the precise characterization of each subcell and of the performance of series-connected solar cells, such as external quantum efficiency (EQE) measurements^{2,3,18–20} and electroluminescence (EL) measurements.²¹ The nonlinear behavior of LC has been pointed out based on a model of the competition between radiative

and non-radiative processes in the luminescent junction.²² To understand the properties of LC effects, an analysis was performed using an optoelectronic model of multi-junction cells.²¹ It indicates that the LC efficiency depends on the device structure²¹ and the properties of bonded interfaces such as air gaps.^{23,24} In addition to bias-voltage dependent luminescence termed as EL coupling,²⁰ photoluminescent (PL) coupling has been indicated as bias-voltage independent luminescence.^{16,20,25} Here, EL and PL are defined as bias-voltage dependent and independent luminescence, respectively. Even though other characterization approaches have been proposed,^{26,27} to the best of our knowledge, LC properties have not been well investigated from the viewpoint of the voltage dependence of a light-emitting subcell.

In series-connected multi-junction cells, the output voltage can be measured only in the two-terminal configuration. This makes it difficult to investigate subcell open-circuit voltages (V_{oc}); doing so requires multiplex measurements and model analysis.^{13,28} EL measurements have been used to obtain the subcell V_{oc} with EQE based on Rau's reciprocity relation.^{29–31} In EL measurements of luminescent multi-junction devices, however, luminescence generates an additional photocurrent in the adjacent lower subcell when a forward-bias voltage is applied to the device, thus preventing precise characterization of the subcell voltages.³² As another approach, transient voltage measurements using pulsed light irradiation have been demonstrated to allow for the evaluation of the internal voltages of individual subcells.^{33–36} The method is beneficial as the evaluation of the subcell voltage is not based on luminescence intensity, which makes the method potentially useful to study the luminescent effect. This method can be used to obtain the voltage in the subcell which is emitting luminescence, and it can be combined with LC current measurements to determine the fundamental LC

^{a)}tayagaki-t@aist.go.jp

properties to understand both the voltage-independent PL and the voltage-dependent EL.³⁷

In this article, we investigate LC properties in multi-junction solar cells by using transient V_{oc} measurements. We study the V_{oc} change under monochromatic illumination to determine the internal voltage of subcells that are emitting luminescence and the impact of LC. In addition, we discuss the impact of unilluminated subcells on voltage measurements in small-sized multi-junction concentrator cells. Moreover, based on the subcell V_{oc} and LC current results, we discuss the voltage dependence of LC properties.

II. EXPERIMENTAL

In this study, we investigate wafer-bonded four-junction GaInP/GaAs//GaInAsP/GaInAs concentrator solar cells with a designated cell area of $A = 0.052 \text{ cm}^2$. The epitaxial structure and fabrication scheme are similar to those published in Refs. 11 and 38. The current-voltage curves and temporal change of V_{oc} are measured under 809-nm laser illumination.^{39,40} The monochromatic irradiance is varied by tuning the laser diode current and using neutral-density filters. Since the GaInP top subcell is transparent for the used laser light and, thus, is expected to generate no photocurrent, the experimental measurements were intentionally conducted using a four-junction cell with a low shunt resistance in the GaInP top subcell. For comparison, also a reference device with a high shunt resistance GaInP subcell was used.

III. RESULTS

A. Luminescent coupling current

Figure 1 shows the optoelectronic equivalent circuit of the series-connected multi-junction solar cell. We label a stack of junctions with the script starting at $i = 1$ following the opposite direction of illumination and name the four subcells J1, ..., J4.

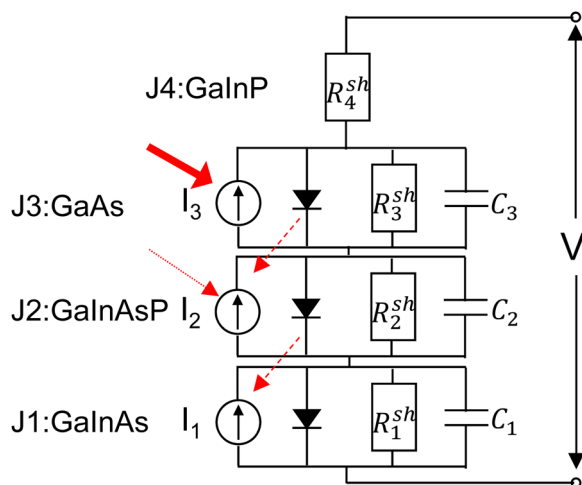


FIG. 1. Schematics of current-voltage measurements under monochromatic illumination and optoelectronic equivalent circuit of the series-connected multi-junction device. The solid red arrows represent laser illumination which is predominantly absorbed by J3. The dashed arrows indicate the light emitted by radiative recombination.

The diode symbols represent the dark current and light-emitting diode. In our experiment, the device is illuminated with 809-nm monochromatic light. The spectral response measurements of J1, J2, J3, and J4 show EQE values of approximately 0%, 4%, 83%, and 0%, respectively, at 810 nm.¹¹ In J4, current flow through this subcell is facilitated by the low shunt resistance. However, regarding J1, this is not the case. Thus, any detected photocurrent of the whole device under 809 nm laser light can be considered as photocurrent generated in J1 by LC from J2 and J3. Figure 2 shows the current-voltage curves of the GaInP/GaAs//GaInAsP/GaInAs four-junction devices measured using a single Xe flash lamp simulator.¹¹ Compared with the reference device with high shunt resistance J4, the device used in the transient V_{oc} measurements shows a reduced fill factor, reflecting primarily the low shunt resistance of J4. From the current reduction with voltage at the arrow, a resistance of about 500Ω can be extracted, which is consistent with the resistance obtained from EL measurements (see Sec. III B).

Figure 3(a) shows the current-voltage curves measured under monochromatic illumination (809 nm) with varying light intensity. Current-voltage curve measurements are performed within 1 ms after 0.2 ms initial illumination by the laser. Although the short-circuit current (I_{sc}) increases with light intensity, the current-voltage curves show a highly tilted slope close to the open-circuit conditions. This behavior can be attributed to the unilluminated J4; the shunt resistance of this subcell acts as an effective series resistance for the remaining three-junction GaAs/GaInAsP/GaInAs device in the two-terminal measurement configuration [Fig. 1].

Figure 3(b) shows the measured short-circuit current I_{sc} as a function of the monochromatic light intensity (red squares). As I_{sc} increases with light intensity, the slope

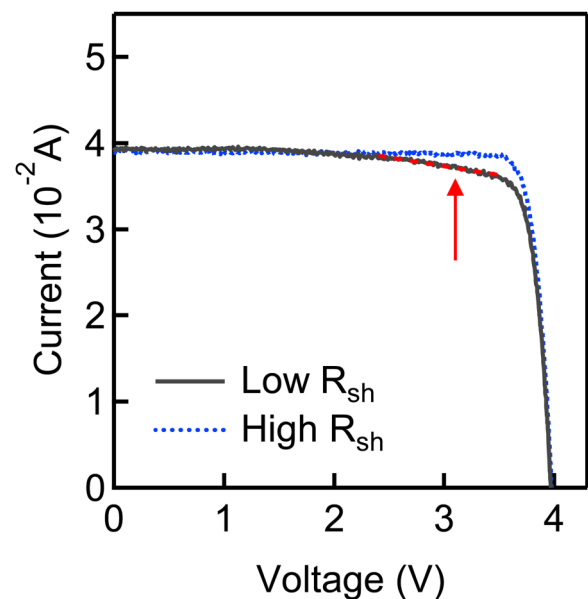


FIG. 2. Current-voltage curves under broadband flash illumination of the investigated device used in this work with low J4 shunt resistance (solid black) and the reference device with a high J4 shunt resistance (dotted blue). The dashed red line represents a linear fit through the shunt-dominated region.

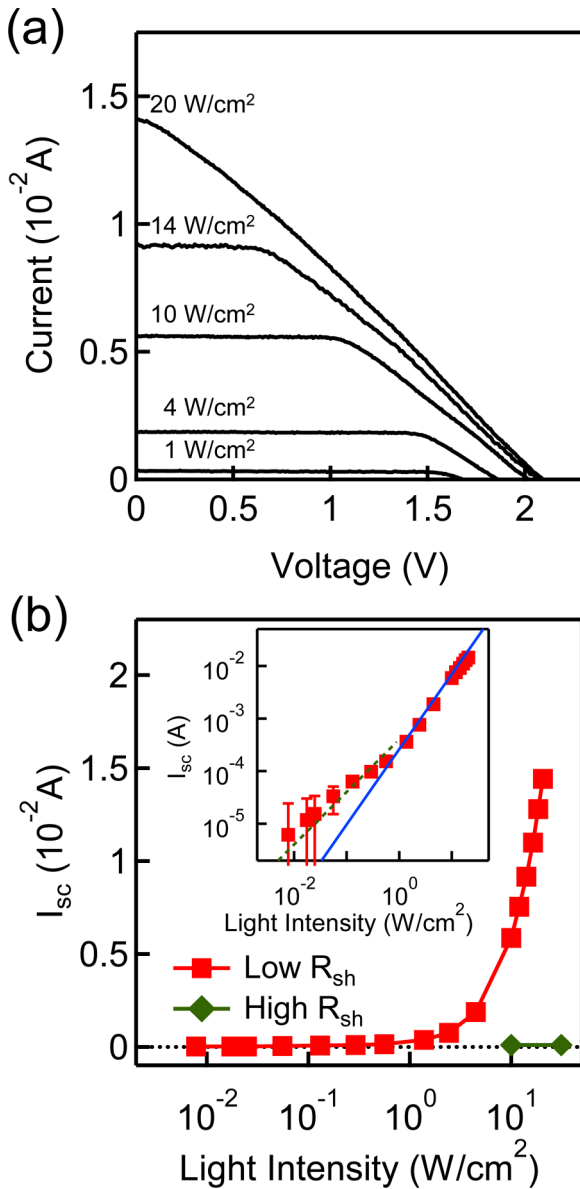


FIG. 3. (a) Current-voltage curves of the device with low J4 shunt resistance measured under 809 nm laser light for different irradiances. (b) Short-circuit current measured under 809 nm laser light of the device used in this work (red squares) and the reference device (green diamonds) as a function of irradiance. Inset: Log-scale. Error bars represent the temporal variation during illumination (see in the text). The dashed and solid lines indicate a result fitted using a linear function and power law, respectively.

changes at approximately 1 W/cm². The increase in measured I_{sc} of the device actually represents an increase in the current in J1, because this subcell limits the current in the series-connected GaAs/GaInAsP/GaInAs device under 809-nm light illumination. This is consistent with the fact that the 809-nm laser light is absorbed predominantly by J3 and partially by J2. Thus, only small LC currents below 0.02 A are generated in J1. For comparison, I_{sc} is measured in the reference device with high shunt resistance J4 [green diamonds in Fig. 3(b)]; it shows barely measurable current even under highest light intensities above 10 W/cm². This indicates that the unilluminated J4's high shunt resistance prevents current flow through the series-connected multi-junction device.

The inset in Fig. 3(b) shows that at low light intensities, I_{sc} increases linearly with light intensity. Above 1 W/cm², I_{sc} increases superlinearly and the current follows the power law with an exponent of approximately 1.43. The transition from linear to superlinear behavior indicates a bias-voltage dependent LC,³⁷ which will be discussed and explained in Sec. IV B and Fig. 7.

B. Electroluminescence measurements

Spectral EL measurements are performed to obtain insight into the current-voltage characteristics of each subcell. Figure 4(a) shows the typical EL spectrum of the GaInP/GaAs//GaInAsP/GaInAs device. EL spectra were measured using a calibrated spectroradiometer.³⁰ EL spectra show almost the same spectral shape for the device with low shunt resistance and the reference device with high shunt resistance. The voltage in each subcell at a given current is

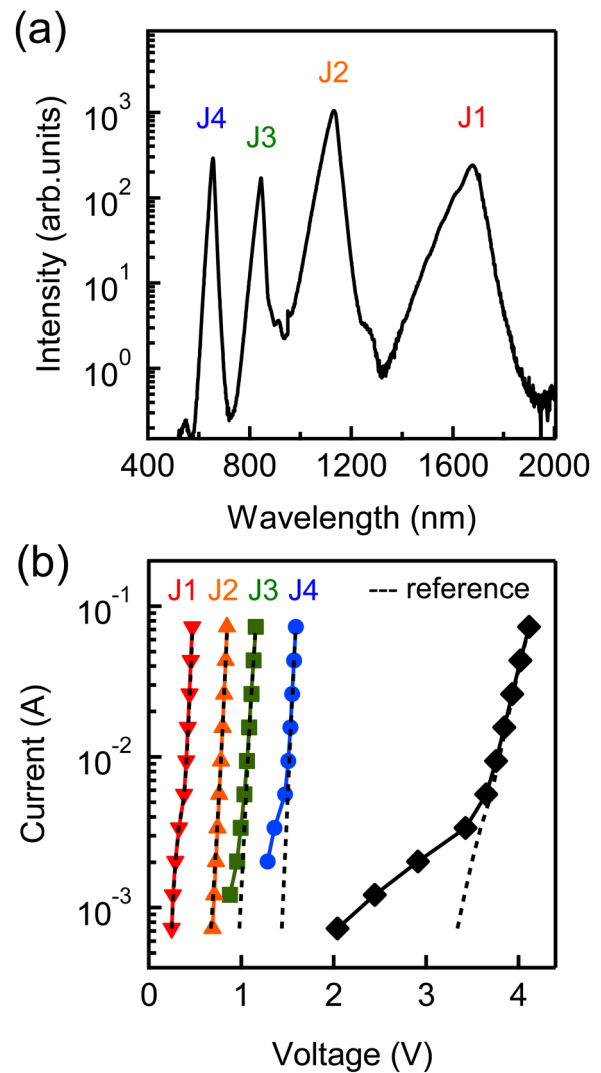


FIG. 4. (a) Typical EL spectra in a GaInP/GaAs//GaInAsP/GaInAs four-junction device. (b) Current-voltage curves under dark condition (black diamonds) and current-voltage curves of each subcell as derived from EL intensity together with EQE: J1 (GaInAs, red inverted triangles), J2 (GaInAsP, orange triangles), J3 (GaAs, green squares), and J4 (GaInP, blue circles). Broken curves indicate the current-voltage curves of the reference device with high J4 shunt resistance.

estimated from the EL intensity by following the procedures reported elsewhere.²⁹ Previous studies have discussed the impact of optical coupling on EL measurements²¹ and pointed out that the resulting correction to the subcell V_{oc} is minimal (<10 mV).³² Using a similar procedure, we estimated the impact of the LC on the subcell voltage to be less than 40 mV, which does not cause a significant influence on the model simulation of transient V_{oc} in Sec. IV A.

Figure 4(b) shows the current-voltage characteristics of each subcell, as derived from this procedure. Note that these data represent I_{sc} - V_{oc} pairs and therefore is free of influences of series resistance.³¹ The enhanced current in J4 at lower voltages indicates its low shunt resistance. The current-voltage characteristics of the reference device with high shunt resistance are shown by the dashed lines in Fig. 4(b). For the model analysis shown later, the current-voltage characteristics are fitted using a single diode model with shunt resistance R_{sh}

$$I_{EL,i}(V_i) = I_{0,i} \left[\exp\left(\frac{qV_i}{m_i kT}\right) - 1 \right] + \frac{V_i}{R_{sh,i}},$$

where I_0 and m are the saturation current and ideality factor, respectively. The obtained parameters are listed in Table I. The shunt resistance obtained for J4 is consistent with the resistance estimated from Fig. 2.

C. Transient V_{oc} measurements

Figure 5(a) shows typical V_{oc} transients after turning on the laser at different light intensities for a pulse duration of 4 ms. The internal resistance of the transient measurement electronics is 2 M Ω . Note that the measurement started only after about 0.1 ms of illumination owing to the limitation of the measurement equipment. At the lowest illumination intensity, V_{oc} increases and then saturates at about 0.3 V. With increasing illumination intensity, the voltage change over time immediately after illumination increases and V_{oc} reaches higher voltages after saturation.

Figure 5(b) shows V_{oc} data taken at 0.2 and 1.2 ms after illumination from Fig. 5(a) as a function of the illumination intensity. With an increase in illumination intensity of up to $\sim 10^{-2}$ W/cm², the V_{oc} increases to ~ 1.3 V, which can be attributed to the photovoltage of J2 and J3 under illumination. Note that the error bars in the inset of Fig. 3(b) reflect the current variation during current-voltage curve measurements as V_{oc} increases gradually with illumination time under low illumination intensity. At higher illumination intensities above $\sim 10^{-2}$ W/cm², V_{oc} increases further with a gradual slope. Under high illumination (>0.1 W/cm²), the

TABLE I. Parameters obtained from EL measurements.

Junction	I_0 (A)	m	R_{sh} (Ω)
J1	4.2×10^{-6}	2.03	>5000
J2	2.4×10^{-13}	1.25	>10000
J3	1.9×10^{-13}	1.69	700
J4	8.7×10^{-22}	1.35	500

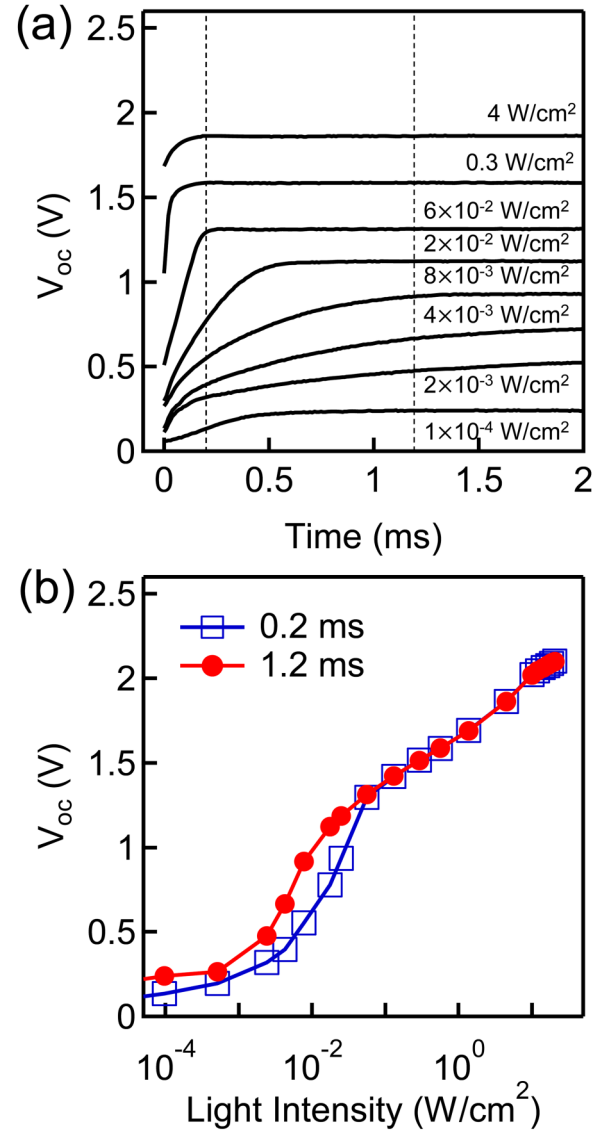


FIG. 5. (a) Measured temporal change of the V_{oc} for different illumination intensities in GaInP/GaAs//GaInAsP/GaInAs devices. (b) Measured V_{oc} shortly after illumination as a function of light intensity, plotted for values at 0.2 and 1.2 ms after starting measurements.

voltage increases logarithmically and follows well the voltage behavior expected from the one-diode model as

$$V_{oc} = \frac{mk_B T}{q} \ln\left(\frac{I_{sc}}{I_0} + 1\right), \quad (1)$$

where I_{sc} is proportional to the illumination intensity.

IV. DISCUSSION

A. Model simulation of transient V_{oc}

It is crucial to determine the subcell voltages for understanding the voltage dependence of the LC. To understand the subcell voltages generated under monochromatic illumination, we model the transient V_{oc} under varying light intensity. Here, we assume the series-connected subcells as one-diode models with photocurrent source, diode, shunt resistance, and an additional parallel capacitance [Fig. 1],

instead of a more complete circuit model.⁴² In a series-connected multi-junction solar cell, the subcell photocurrents can be written as a sum of the photocurrent generated by external illumination (I_{photo}) and the internal illumination (I_{EL}) due to LC from EL emission in subcell(s) above, respectively

$$I_i(t) = I_{\text{photo},i}(t) + \alpha_{ji} I_{\text{EL},j}(V_j), \quad (2)$$

where α_{ji} is the LC efficiency from the j th to the i th subcell. The photocurrent is proportional to the illumination intensity. The current in each subcell $I_{\text{subcell},i}(t)$ is determined as

$$I_{\text{subcell},i}(t) = I_i(t) - I_{0,i} \left[\exp\left(\frac{qV_i(t)}{m_i kT}\right) - 1 \right] - \frac{V_i(t)}{R_{sh,i}} - C_i \frac{dV_i(t)}{dt}, \quad (3)$$

where $I_{0,i}$, m_i , $R_{sh,i}$, and C_i are the saturation current of the diode, ideality factor, shunt resistance, and capacitance, respectively, of the i th subcell. For simplicity, the capacitance is assumed to be independent of the photocurrent. In addition, even though the subcell current $I_{\text{subcell},i}(t)$ is zero under ideal open-circuit conditions, in practice, it is not zero because of the current flow via the resistance of the measurement-device used for voltage measurements: $I_{\text{subcell},i}(t) = V_{\text{meas}}(t)/R_{\text{meas}}$, where $V_{\text{meas}}(t)$ and R_{meas} are the measured output voltage and device resistance, respectively. Thus, Eq. (3) must be extended by this term. Rearranging gives

$$\frac{dV_i(t)}{dt} = \frac{I_i(t)}{C_i} - \frac{I_{0,i}}{C_i} \left[\exp\left(\frac{qV_i(t)}{m_i kT}\right) - 1 \right] - \frac{V_i(t)}{C_i R_{sh,i}} - \frac{V_{\text{meas}}(t)}{C_i R_{\text{meas}}}. \quad (4)$$

The total output voltage is calculated as $V(t) = \sum_{i=1}^4 V_i(t)$, where $V_i(t)$ is the voltage of the i th subcell.

Assuming $I_{\text{photo},i}$ proportional to the laser intensity and the EQE at ~ 810 nm, C and R_{meas} of the device to be 100 nF and 2 M Ω , respectively, and using the EL intensity $I_{\text{EL},j}$ from the EL measurements shown in Fig. 4(b), we can apply this model to calculate the temporal V_{oc} profile. Here, we assume for simplicity time- and intensity-independent values for the capacitance C . In addition, to reproduce the transient V_{oc} under medium light intensities as well as possible, we used a fixed value of 100 nF while the capacitance is typically around 100 nF/cm² and depends on the applied voltage and light intensity.^{33,41} The LC efficiencies are set to 0.1 for the coupling from both J3-to-J2 and J2-to-J1 ($\alpha_{32} = \alpha_{21} = 0.1$) while coupling from J3-to-J1 was set to zero. This is supported by the fact that the coupling efficiency from J3-to-J1 is estimated as $\alpha_{31} \approx \alpha_{21} \times \alpha_{32} = 0.01$ for the case of $\alpha_{32} = \alpha_{21} = 0.1$. Note that in the experiments using realistic devices, the coupling efficiencies may depend on illumination intensity and applied voltage and, as a result, on time as well. Figure 6(a) shows these calculated profiles of the total V_{oc} for different illumination intensities. At low illumination intensity of 8×10^{-3} W/cm², J3 generates a photovoltage. The voltage increases and the slope starts to decrease with illumination time. The time required to reach the saturation

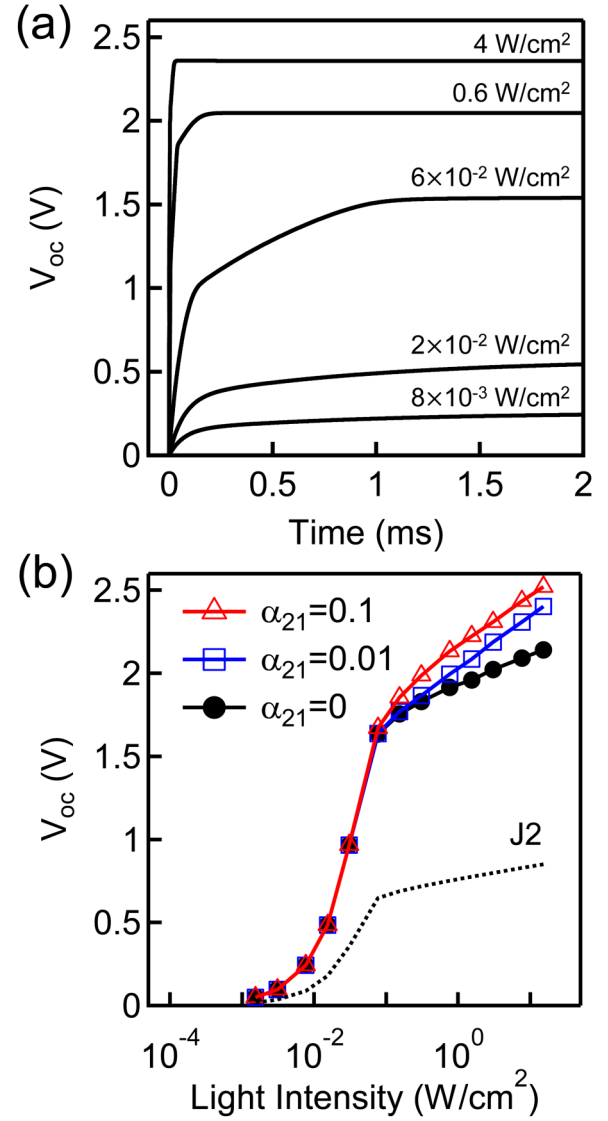


FIG. 6. Temporal change of V_{oc} for (a) the reference device with high shunt resistance J4 and (b) the device with low shunt resistance J4. For each case, two profiles are plotted, which were obtained using measurement equipment with different internal resistance R_{meas} of 2 M Ω (solid curve) and 0.2 M Ω (broken curves). The laser intensity is plotted as red lines in the top. It was switched on in continuous wave mode and turned off after ~ 0.8 ms.

voltage depends on the voltage increase over time, which is determined by illumination intensity and capacitance as indicated by Eq. (4). Under medium illumination intensity, J3 voltage increases rapidly to ~ 1 V. Then, J2 shows a gradual increase in the voltage that originates both from direct laser illumination to J2 and LC from J3. Higher illumination intensity results in an increase in the voltage in J1 owing to the LC from J2 only (no absorption of external illumination in J4). The voltages themselves are either too low (at 8×10^{-3} W/cm²) or too high (at 4 W/cm²) compared to the experiment [Fig. 5(a)]. This is likely related to the LC efficiency α_{ij} , being chosen as fixed value whereas in reality, these LC efficiencies change depending on light intensity and internal voltage applied to the subcells as discussed in Fig. 7.

Figure 6(b) shows the simulation results of the total V_{oc} at 2 ms for different LC efficiencies α_{21} as a function of the illumination intensity. The LC efficiency for the coupling

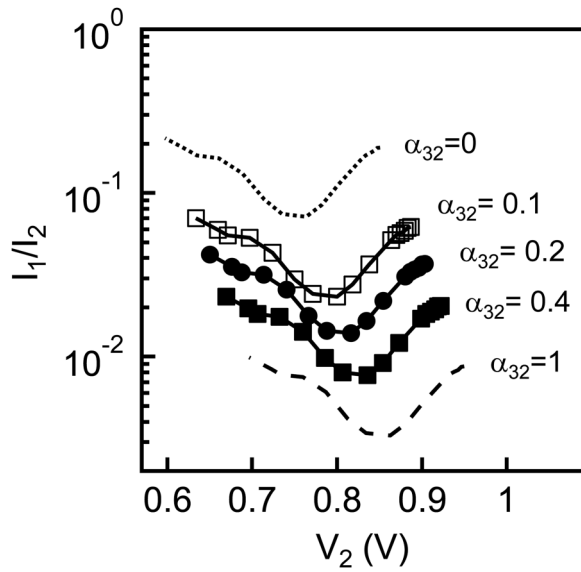


FIG. 7. (a) Simulation results of the total V_{oc} transients for different light intensities with LC. The LC efficiencies were set as $\alpha_{32} = \alpha_{21} = 0.1$. (b) Simulation results of the total V_{oc} at 2 ms for different LC efficiencies α_{21} as a function of light intensity ($\alpha_{21} = 0.1$ kept constant). The dotted curve shows the calculated J2 voltage.

from J3-to-J2 is set to 0.1 ($\alpha_{32} = 0.1$). For zero LC ($\alpha_{21} = 0$), the V_{oc} change over time is determined only by J2 and J3, whereas the V_{oc} increases with steeper slope due to the appearance of LC above 0.1 W/cm^2 for a LC efficiency of $\alpha_{21} = 0.01$, and even more pronounced for $\alpha_{21} = 0.1$. The V_{oc} increase with illumination intensity follows the sum of the J1, J2, and J3 voltages. Note that under low light intensities, the V_{oc} remains zero, which differs from the experimental curves. This is probably due to the larger capacity assumed in the model.

While the measured V_{oc} follows the expected logarithmic increase, the absolute values in Fig. 5(b) show a lower V_{oc} compared to the calculated V_{oc} in Fig. 6(b). As a possible cause for this lower voltage, the potential influence of a counter-voltage in the unilluminated subcell^{33,34} is discussed in the Appendix. As a result, it is concluded that the counter-voltage effect is unlikely to cause the lower voltages in Fig. 5(b). As another possible cause, a recent study has pointed out the influence of the diffusion capacitance on the voltage measurements.⁴¹ Under forward-bias voltages, the diffusion capacitance, which is proportional to the photocarrier concentration in the diode, may increase significantly under illumination. The diffusion capacitance is also proportional to the current flow across the diode, which causes the V_{oc} reduction.⁴¹ Enhanced diffusion capacitance can prevent the increase in voltage even under strong illumination. More quantitative studies on the capacitance are necessary to clarify the cause, however, this is beyond the scope of this work.

Even though the absolute values between the experimental results in Fig. 5(b) and the calculated results in Fig. 6(b) differ, the slope above 0.1 W/cm^2 of the experimental result remains almost unchanged up to 10 W/cm^2 , where a LC current is generated in J1 in Fig. 3(b). These indicate that a part of the obtained V_{oc} originates from J1 even at illumination

intensity $\sim 0.1 \text{ W/cm}^2$ in Fig. 5(b). This is consistent with the assignment that the current increase in Fig. 3(b) corresponds to an increase in minority carriers generated in J1 owing to LC under strong illumination. In addition, the calculated J2 voltages are shown by the dotted curve in Fig. 6(b). The subcell voltage also increases logarithmically under high illumination ($>0.1 \text{ W/cm}^2$), which indicates that the J2 voltage increases monotonously with illumination intensity as Eq. (1). Here, we note that the calculated values of the J2 voltage may be overestimated as the difference between the experimental results in Fig. 5(b) and the calculated results in Fig. 6(b) but logarithmic increase in voltage under high illumination can be reproduced well by the model.

B. Properties of LC efficiency

Finally, we discuss the LC properties based on the obtained results. In particular, we analyze the voltage dependence of the LC efficiency from J2 to J1 α_{21} . We calculated the J2's current I_2 for different light intensities using Eq. (2) for different values for the LC efficiency between J3 and J2 α_{32} . The J2's voltage V_2 is calculated using the calculated I_2 and Eq. (1). Note that the calculated V_2 values may be overestimated as the difference between the experimental and calculated voltage curves in Figs. 5 and 6. The current increase in Fig. 3(b) reflects an increase in J1's current I_1 because this subcell limits the current in the series-connected multi-junction device (assuming that J4 is basically shunted). Then, we obtained the current ratio I_1/I_2 that reflects the LC efficiency α_{21} .

Figure 7 shows this current ratio I_1/I_2 as a function of the J2 voltage V_2 . Since I_2 increases with α_{32} , the calculated I_1/I_2 decreases with increasing α_{32} . As a result, while for low LC efficiency of $\alpha_{32} = 0.1$, the I_1/I_2 varies in a range $0.02 - 0.07$, the I_1/I_2 decreases to less than 0.01 for $\alpha_{32} = 0.4$. In addition, an increase in I_2 with α_{32} results in a voltage increase in J2. $I_1/I_2 - V_2$ curve shifts by 100 mV for an increase in α_{32} from 0 to 1. Furthermore, the I_1/I_2 decreases with increasing V_2 and then increases again with further increase in bias voltage, which indicates that the LC coupling efficiency α_{21} depends on the internal voltage of the subcell that emits luminescence. Because the internal voltage applied to the light-emitting J2 increases with illumination intensity, the I_1 increases linearly at low illumination and superlinearly at higher illumination in Fig. 3(b), corresponding to low and high internal voltages applied to the light-emitting J2, respectively. The LC current in J1 originates from the radiative recombination current in J2. Therefore, the voltage-dependent LC efficiency α_{21} means that the radiative fraction in the current in J2 decreases and increases with the subcell voltage. As a possible mechanism, a theoretical study³⁷ has predicted such voltage-dependent coupling and explained it as follows. At low voltages, even though the subcell current is negligibly small and no EL appears, the radiative recombination of minority carriers emits PL.¹⁶ The PL of higher-bandgap subcells is coupled to lower-bandgap subcells as well as EL, which leads to LC current. At intermediate ranges, minority carriers in the light-emitting subcell favor a non-radiative path that causes lower LC efficiency. In contrast, LC increases

at high voltages because of enhanced radiative recombination in the light-emitting subcell. In conclusion, the superlinear increase in current at higher illumination represents LC caused by EL, whereas the linearly increased current at low illumination reflects the presence of PL, indicating that voltage-independent PL occurs even when the subcell is not yet emitting EL.

V. SUMMARY

We investigated the LC in multi-junction GaInP/GaAs//GaInAsP/GaInAs concentrator solar cells by using transient V_{oc} measurements under monochromatic illumination. We discussed the subcell V_{oc} from the V_{oc} profiles for different illumination light intensities. From the LC current and subcell V_{oc} analysis, we found that LC occurs from J2 to J1. Furthermore, in light of photo- and electroluminescence processes, we showed that LC effects depend on the subcell voltage, reflecting that the radiative recombination rate in the light-emitting subcell varies with the internal subcell voltage.

This approach provides an opportunity to investigate LC properties from the viewpoint of the voltage dependence of a light-emitting subcell. A benefit of the described method is that the evaluation of the subcell voltage is not based on luminescence intensity, which is different from a conventional method using EL measurements and that it is potentially useful to study luminescence effects. This transient V_{oc} measurement can be applied to investigate the LC in various kinds of multi-junction devices, including also III-V/Si multi-junction solar cells^{43–46} and perovskite/Si tandem solar cells,^{47–50} where Si bottom subcells may limit the current.

ACKNOWLEDGMENTS

The authors gratefully acknowledge M. Schachtner and A. Wekkeli for their experimental support. The authors gratefully acknowledge the contributions to the development and fabrication of the four-junction device of A. W. Bett, P. Beutel, F. Dimroth, M. Grave, C. Karcher, E. Oliva, M. Schachtner, T. N. D. Tibbits, and A. Wekkeli, as well as C. Drazek, E. Guiot, T. Signamarcheix, and A. Tauzin. T.T. acknowledges a AIST fellowship for international research, the New Energy and Industrial Technology Development Organization (NEDO) under the Ministry of Economy, Trade and Industry (METI), and KAKENHI (Grant No. 18K07987) from JSPS.

APPENDIX: COUNTER-VOLTAGE EFFECTS IN UNILLUMINATED SUBCELL

As a possible cause for the lower voltage in Fig. 5(a), we study the potential influence of a counter-voltage in the unilluminated subcell.^{33,34} Note that a larger subcell shunt resistance in smaller-sized devices may cause a higher influence to voltage measurements: the device size of the concentrator solar cells used here is around three orders of magnitude smaller than that of solar cells used in previous studies.^{33–36} Figure 8(a) shows the transient V_{oc} under 1-ms pulsed illumination in the reference device with high shunt resistance J4 obtained for measurement-device resistance of 2

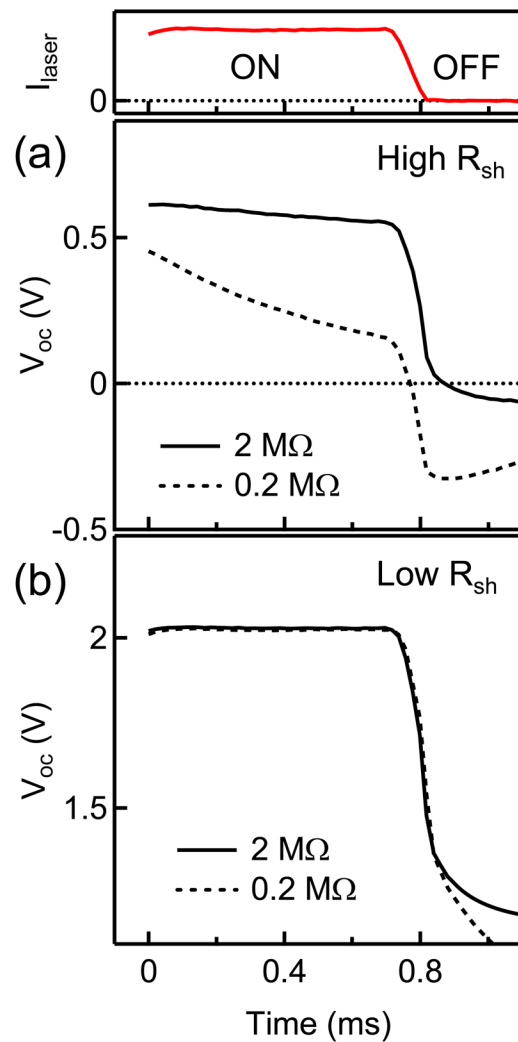


FIG. 8. Extracted current ratio I_1/I_2 for J1 to J2 as a function of V_2 for different assumed LC efficiencies α_{32} .

and 0.2 M Ω . For the reference device, a significant difference appears between measurements with different measurement-device resistances. When the shunt resistance in the unilluminated subcell is high and comparable to the internal resistance of voltage measurement equipment, the measured voltage is reduced by the counter-voltage effect in the unilluminated J4. This effect is caused by the high subcell resistance and non-negligible current flowing through the measurement equipment even at “open-circuit” condition. Measured voltages are reduced even by a small current flow, which causes a large voltage reduction in the subcell with high resistance. Figure 8(b) shows the transient V_{oc} in the device with the low shunt resistance J4. In contrast to the reference device, the transient V_{oc} is almost identical for both resistances, showing that for this device, the measured voltage is less affected by a counter-voltage in the unilluminated subcell.

¹D. J. Friedman, J. F. Geisz, and M. A. Steiner, *IEEE J. Photovoltaics* **4**, 986 (2014).

²A. S. Brown and M. A. Green, in *Proceedings 29th IEEE Photovoltaics Specialists Conference* (IEEE, 2002), p. 868.

- ³C. Baur, M. Hermle, F. Dimroth, and A. W. Bett, *Appl. Phys. Lett.* **90**, 192109 (2007).
- ⁴G. Letay, M. Hermle, and A. W. Bett, *Prog. Photovoltaics Res. Appl.* **14**, 683 (2006).
- ⁵B. M. Kayes, H. Nie, R. Twist, S. G. Spruytte, F. Reinhardt, I. C. Kizilyalli, and G. S. Higashi, in *Proceedings of the 37th IEEE Photovoltaic Specialists Conference* (IEEE, 2011), p. 4.
- ⁶O. D. Miller, E. Yablonovitch, and S. R. Kurtz, *IEEE J. Photovoltaics* **2**, 303 (2012).
- ⁷M. A. Steiner, J. F. Geisz, I. Garcia, D. J. Friedman, A. Duda, and S. R. Kurtz, *J. Appl. Phys.* **113**, 123109 (2013).
- ⁸A. W. Walker, H. Oliver, D. N. Micha, B. Bl, A. W. Bett, and F. Dimroth, *IEEE J. Photovoltaics* **5**, 1636 (2015).
- ⁹V. Ganapati, M. Steiner, and E. Yablonovitch, *IEEE J. Photovoltaics* **6**, 801 (2016).
- ¹⁰C. L. Schilling, O. Hohn, D. N. Micha, S. Heckelmann, V. Klinger, E. Oliva, S. W. Glunz, and F. Dimroth, *IEEE J. Photovoltaics* **8**, 348 (2018).
- ¹¹F. Dimroth, T. N. D. Tibbits, M. Niemeyer, F. Predan, P. Beutel, C. Karcher, E. Oliva, G. Siefert, D. Lackner, P. Fus-Kailuweit, A. W. Bett, R. Krause, C. Drazek, E. Guiot, J. Wasselin, A. Tauzin, and T. Signamarcheix, *IEEE J. Photovoltaics* **6**, 343 (2016).
- ¹²H. Yoon, R. King, R. Richard, G. S. Kinsey, S. Kurtz, and D. D. Krut, in *Proceeding 3rd World Conference on Photovoltaic Energy Conversion* (IEEE, 2003), Vol. 1, p. 745.
- ¹³D. Friedman, J. F. Geisz, and M. A. Steiner, *IEEE J. Photovoltaics* **3**, 429 (2013).
- ¹⁴B. M. Kayes, L. Zhang, R. Twist, I.-K. Ding, and G. S. Higashi, *IEEE J. Photovoltaics* **4**, 729 (2014).
- ¹⁵A. W. Walker, O. Höhn, D. N. Micha, L. Wagner, H. Helmers, A. W. Bett, and F. Dimroth, *J. Photon. Energy* **5**, 053087 (2015).
- ¹⁶D. Lan, J. F. Geisz, M. A. Steiner, I. Garcia, D. J. Friedman, and M. A. Green, *Sol. Energy Mater. Sol. Cells* **143**, 48 (2015).
- ¹⁷M. Steiner, G. Siefert, T. Hornung, G. Peharz, and A. W. Bett, *Prog. Photovoltaics Res. Appl.* **23**, 385 (2015).
- ¹⁸S. H. Lim, J.-J. Li, E. H. Steenbergen, and Y.-H. Zhang, *Prog. Photovoltaics Res. Appl.* **21**, 344 (2013).
- ¹⁹M. A. Steiner, J. F. Geisz, T. E. Moriarty, R. M. France, W. E. McMahon, J. M. Olson, S. R. Kurtz, and D. J. Friedman, *IEEE J. Photovoltaics* **3**, 879 (2013).
- ²⁰D. Lan and M. A. Green, *Appl. Phys. Lett.* **106**, 263902 (2015).
- ²¹J. F. Geisz, M. A. Steiner, R. M. France, W. E. McMahon, C. R. Osterwald, and D. J. Friedman, *IEEE J. Photovoltaics* **5**, 1827 (2015).
- ²²M. A. Steiner and J. F. Geisz, *Appl. Phys. Lett.* **100**, 251106 (2012).
- ²³V. Ganapati, C.-S. Ho, and E. Yablonovitch, *IEEE J. Photovoltaics* **5**, 410 (2015).
- ²⁴T. Tayagaki, K. Makita, H. Mizuno, and T. Sugaya, *J. Appl. Phys.* **122**, 23101 (2017).
- ²⁵D. Lan and M. A. Green, *Prog. Photovoltaics Res. Appl.* **24**, 1566 (2016).
- ²⁶T. Sogabe, A. Ogura, C. Y. Hung, V. Evstropov, M. Mintairov, M. Shvarts, and Y. Okada, *Appl. Phys. Lett.* **103**, 263907 (2013).
- ²⁷D. F. Marrón, E. Barrigón, M. Ochoa, and I. Artacho, *Phys. Rev. Appl.* **6**, 14001 (2016).
- ²⁸T. Tayagaki, K. Makita, H. Mizuno, R. Oshima, and T. Sugaya, *Jpn. J. Appl. Phys.* **56**, 08MC01 (2017).
- ²⁹T. Kirchartz, U. Rau, M. Hermle, A. W. Bett, A. Helbig, and J. H. Werner, *Appl. Phys. Lett.* **92**, 123502 (2008).
- ³⁰S. Roensch, R. Hoheisel, F. Dimroth, and A. W. Bett, *Appl. Phys. Lett.* **98**, 25113 (2011).
- ³¹C. Karcher, H. Helmers, M. Schachtner, F. Dimroth, and A. W. Bett, *Prog. Photovoltaics* **22**, 757 (2014).
- ³²J. F. Geisz, R. M. France, I. García, M. A. Steiner, and D. J. Friedman, *AIP Conf. Proc.* **1616**, 114 (2014).
- ³³H. Nesswetter, N. R. Jost, P. Lugli, A. W. Bett, and C. G. Zimmermann, *Appl. Phys. Lett.* **106**, 23903 (2015).
- ³⁴M. Rutzinger, H. Nesswetter, P. Lugli, A. W. Bett, and C. G. Zimmermann, *Appl. Phys. Lett.* **108**, 253902 (2016).
- ³⁵M. Rutzinger, M. Salzberger, H. Nesswetter, D. Lackner, A. W. Bett, P. Lugli, and C. G. Zimmermann, *IEEE J. Photovoltaics* **7**, 709 (2017).
- ³⁶H. Nesswetter, N. R. Jost, P. Lugli, A. W. Bett, and C. G. Zimmermann, *Prog. Photovoltaics Res. Appl.* **24**, 760 (2016).
- ³⁷J. Jia, Y. Miao, Y. Kang, Y. Huo, M. Mazouchi, Y. Chen, L. Zhao, H. Deng, P. Supaniratsai, S. H. AlQahtani, and J. S. Harris, *Opt. Express* **23**, A219 (2015).
- ³⁸F. Dimroth, M. Grave, P. Beutel, U. Fiedeler, C. Karcher, T. N. D. Tibbits, E. Oliva, G. Siefert, M. Schachtner, A. Wekkeli, A. W. Bett, R. Krause, M. Piccin, N. Blanc, C. Drazek, E. Guiot, B. Ghyselen, T. Salvétat, A. Tauzin, T. Signamarcheix, A. Dobrich, T. Hannappel, and K. Schwarzburg, *Prog. Photovoltaics Res. Appl.* **22**, 277 (2014).
- ³⁹S. K. Reichmuth, H. Helmers, C. E. Garza, D. Vahle, M. de Boer, L. Stevens, M. Mundus, A. W. Bett, and G. Siefert, in *Proceedings of the EUPVSEC 2016* (WIP GmbH & Co Planungs-KG, 2016), p. 5.
- ⁴⁰S. K. Reichmuth, H. Helmers, S. P. Philipps, M. Schachtner, G. Siefert, and A. W. Bett, *Prog. Photovoltaics Res. Appl.* **25**, 67 (2017).
- ⁴¹M. Rutzinger, M. Salzberger, A. Gerhard, H. Nesswetter, P. Lugli, and C. G. Zimmermann, *Appl. Phys. Lett.* **111**, 183507 (2017).
- ⁴²D. Lan and M. A. Green, *Prog. Photovoltaics Res. Appl.* **24**, 1566 (2016).
- ⁴³S. Essig, J. Benick, M. Schachtner, A. Wekkeli, M. Hermle, and F. Dimroth, *IEEE J. Photovoltaics* **5**, 977 (2015).
- ⁴⁴H. Mizuno, K. Makita, T. Tayagaki, T. Mochizuki, T. Sugaya, and H. Takato, *Appl. Phys. Express* **10**, 72301 (2017).
- ⁴⁵R. Cariou, J. Benick, P. Beutel, N. Razeq, C. Flotgen, M. Hermle, D. Lackner, S. W. Glunz, A. W. Bett, M. Wimplinger, and F. Dimroth, *IEEE J. Photovoltaics* **7**, 367 (2017).
- ⁴⁶R. Cariou, J. Benick, F. Feldmann, O. Höhn, H. Hauser, P. Beutel, N. Razeq, M. Wimplinger, B. Bläsi, D. Lackner, M. Hermle, G. Siefert, S. W. Glunz, A. W. Bett, and F. Dimroth, *Nat. Energy* **3**, 326 (2018).
- ⁴⁷J. P. Mailoa, C. D. Bailie, E. C. Johlin, E. T. Hoke, A. J. Akey, W. H. Nguyen, M. D. McGehee, and T. Buonassisi, *Appl. Phys. Lett.* **106**, 121105 (2015).
- ⁴⁸J. Werner, B. Niesen, and C. Ballif, *Adv. Mater. Interfaces* **5**, 1700731 (2018).
- ⁴⁹F. Sahli, J. Werner, B. A. Kamino, M. Bräuninger, R. Monnard, B. Paviet-Salomon, L. Barraud, L. Ding, J. J. D. Leon, D. Sacchetto, G. Cattaneo, M. Despeisse, M. Boccard, S. Nicolay, Q. Jeangros, B. Niesen, and C. Ballif, *Nat. Mater.* **17**, 820 (2018).
- ⁵⁰N. Tucher, O. Höhn, B. Bläsi, and J. C. Goldschmidt, *Proc. SPIE* **10688**, 1068805 (2018).